Ballistic-electron-emission spectroscopy of $Al_xGa_{1-x}As/GaAs$ heterostructures: Conduction-band offsets, transport mechanisms, and band-structure effects

J. J. O'Shea, E. G. Brazel, M. E. Rubin, S. Bhargava, M. A. Chin, and V. Narayanamurti*

Materials Department, Physics Department, and Electrical and Computer Engineering Department, University of California, Santa Barbara, California 93106

(Received 11 February 1997)

We report an extensive investigation of semiconductor band-structure effects in single-barrier $Al_xGa_{1-x}As/GaAs$ heterostructures using ballistic-electron-emission spectroscopy (BEES). The transport mechanisms in these single-barrier structures were studied systematically as a function of temperature and Al composition over the full compositional range ($0 \leqslant x \leqslant 1$). The initial ($\Gamma$) BEES thresholds for $Al_xGa_{1-x}As$ single barriers with $0 \leqslant x \leqslant 0.42$ were extracted using a model which includes the complete transmission probability of the metal-semiconductor interface and the semiconductor heterostructure. Band offsets measured by BEES are in good agreement with previous measurements by other techniques which demonstrates the accuracy of this technique. BEES measurements at 77 K give the same band-offset values as at room temperature. When a reverse bias is applied to the heterostructures, the BEES thresholds shift to lower voltages in good agreement with the expected bias-induced band-bending. In the indirect band-gap regime ($x > 0.45$), spectra show a weak ballistic-electron-emission microscopy current contribution due to intervalley scattering through $Al_xGa_{1-x}As$ X valley states. Low-temperature spectra show a marked reduction in this intervalley current component, indicating that intervalley phonon scattering at the $GaAs/Al_xGa_{1-x}As$ interface produces a significant fraction of this X valley current. A comparison of the BEES thresholds with the expected composition dependence of the $Al_xGa_{1-x}As$ Γ, L, and X points yields good agreement over the entire composition range. [S0163-1829(97)04827-3]

I. INTRODUCTION

The invention of the scanning tunneling microscope[1] has spawned a variety of scanning probe microscopy (SPM) techniques which have enabled the study of the structural and electronic properties of materials on length scales previously unattainable. The main advantage of scanning probe techniques is the exceptional lateral resolution imparted by the localization of the probe tip. SPM has potential applications in lithography and information storage on length scales not attainable by conventional photolithography. At the same time, SPM has also led to many important fundamental scientific discoveries. SPM variants in which multiple measurements are made simultaneously are particularly fruitful techniques where new information is being obtained.

One such extension of scanning tunneling microscopy (STM) is ballistic-electron-emission microscopy (BEEM),[2,3] which probes subsurface electronic structure. In conventional STM, a sharp metal tip is brought close to a conducting surface allowing quantum-mechanical tunneling between the two conductors. In the most common mode of STM operation, the tip is scanned across the surface at a given tip-sample voltage while a feedback loop maintains a constant tunneling current (I_t). To first order, this produces a topographical image of the surface—with atomic resolution in some cases. BEEM adds a third contact to STM, a thin metal layer which typically forms a Schottky barrier with a semiconductor sample. The STM tip (emitter) injects electrons across the tunneling gap into the metal (base) layer. If the metal layer is thinner than the inelastic mean free path, some of the electrons will traverse the metal base ballistically, surmount the Schottky barrier, and be collected at the semiconductor substrate (collector). There are two basic modes of BEEM: imaging and spectroscopy. A BEEM current image is made by simultaneously measuring the BEEM current during a topographic STM image acquisition (constant I_t, tip bias). In BEEM spectroscopy or BEES, the BEEM current is measured as the tip-base voltage is ramped at a constant I_t. Thus, the energy dependence of hot carrier transport is probed. The initial application of BEEM was in measuring metal-semiconductor (m-s) Schottky barrier heights (SBH) since no collector current (I_c) will be found until a threshold voltage (which corresponds to the Schottky barrier) is reached.

In BEEM, carriers tunnel from a metal tip into the metal base, and the entire tip-base bias is dropped across the tunneling gap. The third contact allows the energy distribution of injected carriers to be controlled independently of the semiconductor band structure. In contrast to STM of a semiconductor where some of the applied tip bias drops across the semiconductor depletion region, there is no bias-induced band-bending in a BEEM experiment. This is a great advantage when using BEEM to study semiconductor heterostructures since the energy levels of interest are unperturbed by the measurement, and the tip voltage corresponds directly to the energy of injected carriers. The application of BEEM to semiconductor heterostructures was proposed by Henderson *et al.*[4] and has been demonstrated in several systems including InAs/GaAs,[5] Si p-n junctions,[6] AlAs/GaAs,[7] SiGe strained layers,[8] and $Al_xGa_{1-x}As/GaAs$ heterostructures.[9,10] More recently, the capabilities of BEEM have been exploited in studies of dislocations in $In_xGa_{1-x}As/GaAs$,[11] ordered-

 © 1997 The American Physical Society

$Ga_xIn_{1-x}P/GaAs$ heterostructures,[12] InAs quantum dots,[13] and InAs/AlSb heterostructures.[14]

We have previously shown that BEEM spectra from single $Al_xGa_{1-x}As$ barrier samples[9] are consistent with measurements of the $GaAs/Al_xGa_{1-x}As$ conduction-band offset (ΔE_C) in the literature.[15,16] We have also shown the effect of quasibound states in an $Al_xGa_{1-x}As/GaAs$ double-barrier resonant tunneling structure (DBRTS) on the BEEM spectra.[10] This paper provides a systematic study of $Al_xGa_{1-x}As$ single barrier structures over the entire $Al_xGa_{1-x}As$ composition range. This comprehensive study firmly establishes BEES capabilities for studying charge transport processes in semiconductor heterostructures.

In Sec. II, we discuss the modification of the BEEM theory to include transmission across semiconductor heterostructures. After describing the experimental procedures (Sec. III), the importance of a uniform Au/GaAs interface is discussed in Sec. IV. BEEM experiments for low Al concentrations are given in Sec. V. For $x \leqslant 0.45$, $Al_xGa_{1-x}As$ has a direct band gap, and the first threshold in the BEES spectra is due to transport through the $Al_xGa_{1-x}As$ Γ valley. Thus, the shift in the initial BEES threshold with respect to the Au/GaAs Schottky barrier gives ΔE_C. Section VI demonstrates the effect of applying a reverse bias to the sample on the BEES spectra. In Sec. VII, results for $Al_xGa_{1-x}As$ barriers in the indirect regime ($x \geqslant 0.45$) are given, and we show that the BEES spectra cannot be explained by simple, single-band transport. We discuss the intervalley scattering processes which must be considered to account for the observed BEES thresholds. Finally, we summarize the thresholds observed for all samples and correlate them to the $GaAs/Al_xGa_{1-x}As$ band structure in Sec. VIII.

II. THEORY

Since BEEM spectra exhibit thresholds at energies where additional states become available for transport, the primary purpose of BEEM spectroscopy is identifying these thresholds and correlating them to semiconductor band structure. In practice, this is accomplished by fitting measured spectra to theoretical models. A three-step model is usually employed to calculate the BEEM current of a simple m-s structure.[2] The three processes considered are (1) tunneling from the STM tip into the metal base, (2) transport of the injected hot electrons through the base, and (3) transmission across the m-s interface. For tunneling from the STM tip, a planar tunneling formalism is generally assumed.[17] Next, the distribution of hot electrons in the metal base is modified by elastic and inelastic scattering. Finally, transmission across the m-s interface determines whether an electron is collected by the substrate as BEEM current. It is convenient to assume conservation of energy and transverse momentum at the m-s interface even though Au/GaAs is not an epitaxial interface.

For injection into a semiconductor with a single (possibly degenerate) band minimum, fitting requires two adjustable parameters: one for the effective Schottky barrier (V_b) and an amplitude factor which accounts for scattering in the metal and at the m-s interface. Two commonly used models are that of Bell and Kaiser[2] (BK) and that of Ludeke and Prietsch (LP).[18] They differ mainly in the treatment of transmission across the m-s interface. The BK model assumes a step transmission function at the m-s interface while LP include the quantum-mechanical (QM) transmission probability. The LP model gives a $(V-V_b)^{5/2}$ dependence of the BEEM current near threshold compared to a $(V-V_b)^2$ dependence in the BK model. Consequently, the fitted threshold (V_b) depends on the model used; the thresholds are typically ~30–50 mV lower when QM transmission is included (LP model).

To properly describe BEEM experiments on semiconductor heterostructures, a fourth step must be added to account for the transmission coefficient of the heterostructure. Recently, calculations of the spectral shape of single and double barrier structures have been published by Smith and Kogan (SK).[19] Their model includes both the transmission probabilities of the m-s interface and the semiconductor heterostructure. Smith and Kogan showed that the second derivative of the BEEM spectra should reflect the transmission probability of the semiconductor heterostructure. Their calculations gave good agreement with our previous BEEM measurements on $GaAs/Al_{0.42}Ga_{0.58}As$ single- and double-barrier structures.[9,10]

In general, the BEEM current normalized to the tunneling current is calculated using:

$$I_c(V)=RI_t\frac{\int_{E_{z\min}}^{\infty}D(E_z,V)\int_0^{E_{t\max}}F(E)T(E_z,E_t)dE_t dE_z}{\int_0^{\infty}D(E_z,V)\int_0^{\infty}[F(E)-F(E+eV)]dE_t dE_z}, \quad (1)$$

where V is the tip bias, R is an attenuator factor, I_t is the tunneling current, D is the WKB tunneling probability, and F is the Fermi function. The integration limits $E_{z\min}=E_F-e(V-V_b)$ and $E_{t\max}=m_t/(m-m_t)[E_z-E_F+e(V-V_b)]$ are set by transverse momentum conservation. E_F is the Fermi energy in the tip, and m_t (m) is the transverse effective mass in the semiconductor (metal). If an electron has a normal wave-vector component corresponding to a energy lower than $E_{z\min}$, it cannot surmount the Schottky barrier. $E_{t\max}$ accounts for the critical angle[2] beyond which all electrons incident to the m-s interface are reflected. In general, the transmission coefficient for the m-s interface and the semiconductor heterostructure, $T(E_z,E_t)$, is a function of both the normal and lateral energy components. The propagation matrix technique was employed to calculate $T(E_z,E_t)$ for the entire structure including both the m-s interface and semiconductor heterostructure.[20] When $T(E)$ is set to 1, Eq. (1) reverts to the BK model. We will refer to the full transmission probability calculation of Eq. (1) as the $T(E)$ model.

III. EXPERIMENT

All samples were grown by molecular beam epitaxy (MBE) at 580 °C on n^+ GaAs (001) substrates. The $Al_xGa_{1-x}As$ alloy composition and layer thickness were calibrated using reflection high-energy electron diffraction oscillations. Dopant concentrations were calibrated from Hall measurements on previous samples. The semiconductor layer structure is shown in the inset of Fig. 1. Wafers with seven different Al compositions spanning the entire $x=0$ (GaAs) to $x=1$ (AlAs) compositional range were grown. The

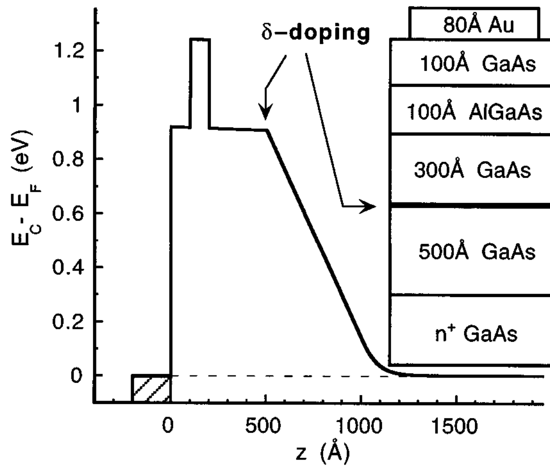

FIG. 1. Calculated band profile for $x=0.42$ $Al_xGa_{1-x}As$ single-barrier assuming a Au/GaAs Schottky barrier of 0.92 eV. $T=300$ K. The δ-doped sheet (Be, 1.1×10^{12} cm^{-2}) was used to flatten the bands. The MBE layer structure is shown in the inset.

structures consist of a 500 Å GaAs buffer layer, a p-type (Be) δ-doped sheet, a 300 Å GaAs spacer layer, a 100 Å $Al_xGa_{1-x}As$ barrier, and a 100 Å GaAs cap layer. The Be sheet doping concentration ($N_A=1.1\times10^{12}$ cm^{-2}) was designed to cancel the band bending near the Schottky barrier, leaving a flat band heterostructure in equilibrium as shown by the calculated band diagram in Fig. 1. Band profiles were calculated self-consistently using the one-dimensional (1D) Poisson/Schroedinger Solver.[21]

To fabricate samples for BEEM, In Ohmic contacts were soldered to the back of the n^+-GaAs substrates. Au Schottky contacts were thermally evaporated at a typical background pressure of 3×10^{-7} Torr. Prior to evaporation, the GaAs surfaces were treated in a 1:5 solution of $NH_4OH:H_2O$ for 90 s followed by a 60 s rinse in deionized water. The Au contacts were nominally 1 mm in diameter and 80–100 Å thick.

We use a Surface/Interface AIVTB-4 variable-temperature STM/BEEM system.[22] Room-temperature (RT) experiments were performed in air. For low-temperature ($77\leqslant T<293$ K) measurements, the STM was placed in a vacuum can ($\sim10^{-6}$ Torr) inside a liquid-nitrogen Dewar. Heat transfer was provided by He exchange gas. The vacuum can provides improved temperature stability and reproducibility compared to immersing the STM in liquid nitrogen. BEEM data were acquired in constant current mode with a 2 nA setpoint unless stated otherwise. BEEM spectra were measured in 2–5 mV steps and signal averaged 50–100 times to improve the signal-to-noise ratio. In some cases, several spectra were averaged and the data points were grouped for clarity.

IV. THE Au/GaAs INTERFACE

We chose $Al_xGa_{1-x}As$/GaAs as the prototypical heterostructure system since it is well controlled as evidenced by its commercial use in quantum well lasers. This enables an essential test or calibration of BEEM heterostructure experiments since the band structures of these materials are relatively well known.[23] All samples have nominally the same Au/GaAs interface formed on an undoped GaAs cap layer. The MBE-grown, undoped cap layer gives a very uniform SBH as measured locally by BEEM, thereby providing an excellent internal energy reference for the heterostructures. Thus, the sample design allows direct assignment of the BEES thresholds to the heterojunction band structure.

The Au/GaAs interface has been the subject of several previous BEEM studies.[2,9,24–28] This interface is known to be reactive;[25] *in situ* deposition of Au on a clean GaAs surface results in a nonuniform interface which degrades electrically over time. Therefore, we prepare our GaAs surfaces chemically which leaves an interfacial oxide layer to prevent interdiffusion and reaction of Au and GaAs. Our surface treatment is similar to that of Talin *et al.*[27] in which an ammonium hydroxide solution is used to etch the GaAs native oxide, then more oxide is formed by rinsing the sample in water. This treatment forms a more uniform interface than using a stronger etch such as HCl followed by the inevitable air exposure while loading the sample for Au deposition.

The Schottky barrier for GaAs is known to depend only slightly on the metal forming the contact, implying that Fermi-level pinning by interface states determines the SBH. Initially, the Au/GaAs interface was studied using a sample containing a 5000 Å undoped GaAs layer grown on an n^+-GaAs substrate. These samples gave BEES thresholds of $\sim$0.9 eV at RT and $\sim$1.0 eV at 77 K. We also performed BEES (using hole injection) on a sample containing a 5000 Å undoped GaAs layer grown on a p^+-GaAs substrate. A slight T dependence in the p-type SBH from 0.52 V at 77 K to 0.51 V at 150 K was found.[29] BEES measurements above 150 K were not possible due to thermionic emission over the barrier. Our BEES results are in excellent agreement with Au/p-type GaAs Schottky barriers measured by conventional current-voltage and capacitance-voltage techniques.[30] Previously, Bell and co-workers[31,32] studied Au/p-type GaAs Schottky barriers by BEEM and found a two-threshold behavior. We also observed two thresholds in our p-type GaAs spectra with a splitting of 0.13 ± 0.02 eV, close to their value of 0.10 ± 0.02 eV.[32] The second threshold has been attributed to the GaAs valence-band structure. At an energy $\sim$0.1 eV below the valence-band maximum, the light-hole band acquires a heavier mass, $m^*=0.5$. This curvature change provides additional states and accounts for the second threshold.

Since the diodes made on the n- and p-type substrates have nominally the same undoped GaAs cap layer and undergo the same preparation, they should have the same Fermi pinning position. Thus, we find that the n-type and p-type SBH's measured by BEES add to the GaAs band gap (E_g) within experimental error. Our measurements show that the Fermi pinning position basically follows the valence-band edge since the T dependence of the n-type SBH accommodates most of the GaAs band-gap T dependence (1.42–1.51 eV from RT to 77 K).

The n-type SBH of 0.9 eV was used to design the samples described in Fig. 1. The GaAs reference sample for all of the following experiments has the same design (with δ doping) as Fig. 1 except that it contains no Al. Hereafter, it will be referred to as ''AL0.'' The BEEM results described below for AL0 are virtually identical to those for the 5000 Å undoped GaAs layer. This ensures that the Au/GaAs interface

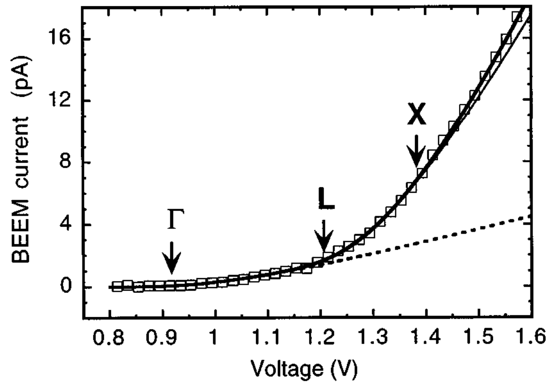

FIG. 2. Typical RT BEEM spectra (points) for Au/GaAs (''AL0'') sample. Least squares fits (lines) to the BK model include current injected into the GaAs Γ, L, and X bands. Thresholds of 0.92, 1.21, and 1.38 eV are found in good agreement with the expected interband energies.

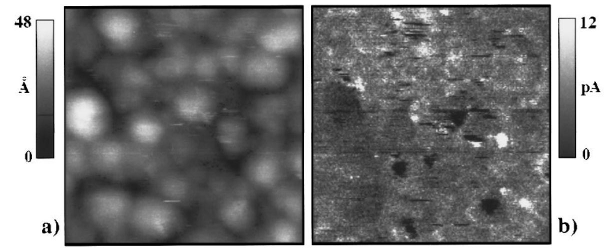

FIG. 3. (a) STM and (b) BEEM image pair of a 1000×1000 Å^2 area of an AL0 sample showing the uniformity of transmission across the Au/GaAs interface. The tunneling current and tip bias were 1 nA and −1.5 V, respectively. The average BEEM current is 5±1 pA.

determines the threshold behavior and that the potential at the δ-doped sheet is equal or slightly less than the Schottky barrier. In other words, the δ-doped layer concentration was designed correctly and has not created a potential barrier (greater than the Schottky barrier) for the injected electrons to overcome. It also indicates the negligible effect of image-force lowering of the Schottky barrier in our experiments.

There is an important difference between the work of Talin *et al.*[28] and our heterostructure experiments regarding the sample design. Their samples were designed to enhance the observation of Schottky barrier nonuniformity by using heavily doped GaAs wafers. In contrast, all Schottky barriers in this study were made on very high quality, MBE-grown, undoped GaAs layers. Palm, Arbes, and Schulz[33] have shown that the distribution of SBH's measured by BEEM depends on the semiconductor doping concentration, and the width of the distribution is much narrower on lower doped samples. Since the unintentional background doping of our material is at most mid-10^{14} cm^{-3} p-type, the characteristic length scale (Debye length) for potential fluctuations of the order of the thermal energy (kT) is ∼1900 Å at RT. The absence of doping minimizes band bending; any local SBH fluctuations will be pinched off[34] and will not be observed by BEES. Furthermore, the p-type, δ-doped sheet also masks any Schottky barrier nonuniformities; a small area with a low SBH will not be detected since the potential maximum would be at the δ-doped sheet, 500 Å inside the semiconductor.

A typical RT BEEM spectra from an AL0 sample is given in Fig. 2. It shows current contributions from injection into the three lowest conduction-band minima (Γ, L, X) of GaAs. The threshold positions, shown by arrows in Fig. 2, were determined by least-squares fitting to the BK model. The total BEEM current is calculated by adding up the contributions from all three bands, and each current component has the form of Eq. (1) with $T(E_z, E_t)=1$. Thresholds are found at 0.92, 1.21, and 1.38 V which correspond to the GaAs Γ, L, and X minima, respectively, in agreement with previous BEEM results.[2] The resulting energy separations between the band minima are also in good agreement with values measured by other techniques.[35] The magnitude and shape of BEEM spectra from AL0 samples and from all other samples described below were consistent and reproducible both for different areas on the same sample and for different diodes from the same wafer.

A strong contribution from the GaAs L valley is observed in agreement with previous reports.[2,28,36,37] This current component is not expected from the simple ballistic picture which predicts a highly forward-directed electron distribution (normal to the interface) at the m-s interface. Assuming transverse momentum (k_t) is conserved at the m-s interface, BEEM thresholds are not expected for band minima which do not project to the zone center of the GaAs (001) interface Brillouin zone. The large L valley current observed implies that k_t is not strictly conserved at the Au/GaAs interface, and the additional k_t is provided by scattering at the m-s interface. Scattering by the interfacial oxide seems likely for our chemically prepared Au/GaAs interfaces.

BEEM imaging was used to study the uniformity of the Au/GaAs interface. Figure 3 shows a STM and BEEM image pair of an AL0 sample taken at RT with a tip bias of −1.5 V and a tunneling current of 1 nA. The 100–200 Å round features in the STM image are the Au grains formed during evaporation. Some correlation between the Au thickness and the BEEM current is seen in the left center of Fig. 3 where a region with less BEEM current (darker) corresponds to a tall Au grain. The average BEEM current in this darker region is 3 pA compared to 5 pA in the area directly above it (upper left corner of the image). The dark spots in the BEEM current image which appear to have zero BEEM current are artifacts due to adsorbates on the Au surface.[38] A histogram of the BEEM image in Fig. 3 (not shown) has an average of 5 pA and a standard deviation of 1 pA. So, the BEEM current is highly uniform over the large majority (∼90%) of the interface.

For heterostructure experiments, a uniform SBH is even more important than uniform BEEM current magnitude. The RT SBH determined from fitting a large number of spectra acquired on many different diodes was 0.915±0.018 V. This value increased to 0.991±0.024 V at 77 K. The increased SBH at low T is expected from the increase in energy gap with decreasing T. The higher-lying L and X thresholds also shift to higher energy at low T as expected. This uniform and reproducible Au/GaAs interface has been utilized in all of the following results.

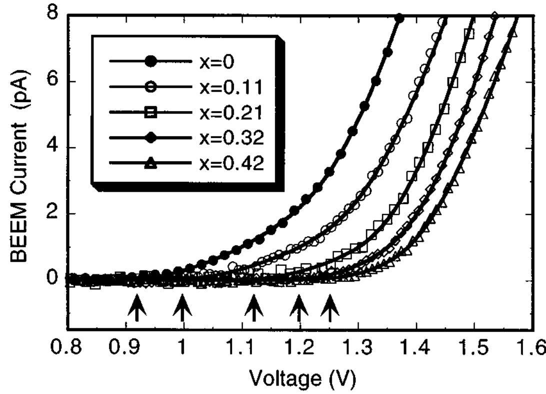

FIG. 4. Comparison of RT BEES spectra (points) for $Al_xGa_{1-x}As$ single barriers. Also shown are BK fits to the data (lines). Note the shift in the initial BEEM threshold (arrows) with Al composition which gives the conduction-band offset.

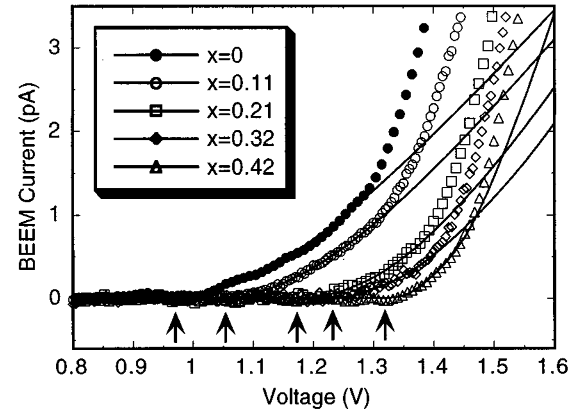

FIG. 5. 77 K BEES spectra comparison for five $Al_xGa_{1-x}As$ compositions. Lines are least-squares fits to a model containing the full transmission probability for the Γ valley. Fitted thresholds are indicated by arrows.

V. DIRECT REGIME ($x \leq 0.42$)—CONDUCTION-BAND OFFSETS

The general approach of these experiments is to systematically vary only the Al composition of the heterostructure. As shown in Fig. 1, the band profiles were engineered (using the δ-doping sheet) to have a flat-band condition in equilibrium at RT. In essence, we have placed a simple potential barrier of variable height (determined by the Al composition) in the path of the injected electrons while keeping all other parameters constant. This ensures that any change in the BEEM spectra must be due to the band structure of the heterojunction barrier. Specifically, the shift in the first (Γ) BEEM threshold compared to the GaAs reference (AL0) sample will give the GaAs/$Al_xGa_{1-x}As$ conduction-band offset.

A comparison of RT BEEM spectra for five different Al compositions is given in Fig. 4. The barrier composition spans the direct gap regime of $Al_xGa_{1-x}As$ (x=0–0.42). The spectra shown are representative of their respective samples. Also shown are fits to the BK model including two thresholds for each sample. The data show a clear increase in the first BEEM threshold with increasing Al content as expected. For the same nominal Au thickness and tunneling current, the magnitude of BEEM current at a given voltage decreases with increasing Al content since more carriers are reflected by the barrier. The additional threshold(s) due to the higher-energy L and X bands also shift with Al composition. Assignments of the higher thresholds to the band structure will be discussed in more detail in Sec. VIII.

In Ref. 9 and Fig. 4, we have used two threshold BK fits to model the $Al_xGa_{1-x}As$ spectra and determined ΔE_C from the difference between the $Al_xGa_{1-x}As$ Γ threshold and the AL0 Γ threshold. Since the sharpness of single-barrier transmission resonances will change with the barrier height, a model which includes the QM transmission across the $Al_xGa_{1-x}As$ barriers should, in principle, be more accurate. However, a model which includes the transmission probabilities of transport through all three bands would require at least six adjustable parameters—three for the $Al_xGa_{1-x}As$ band edges and three amplitude factors. Fitting with so many parameters would not be meaningful as x approaches 0.45 because the three band minima converge. Coupling or scattering between different bands may also be important, but these effects cannot be discerned reliably in this Al composition range due to the degeneracy. As will be shown in Sec. VII, intervalley scattering *must* be used to explain the BEEM threshold due to the X valley in the high Al content structures.

Since we are mainly concerned with ΔE_C, we now consider transport through the Γ valley only using the $T(E)$ model described in Eq. (1). We assume a constant tunneling gap (tip-sample separation), so the integrals in the denominator of Eq. (1) are used to normalize the spectra to the tunneling current at each voltage.[2] In practice, as the voltage is ramped to collect a BEES spectrum, the gap must be adjusted slightly by feedback to maintain a constant I_t. In the SK model, the gap is adjusted at each voltage to give a constant current density. However, assuming a constant tunneling gap over a small voltage range should not greatly affect the shape of the BEEM spectra. One other slight difference between the SK and $T(E)$ models is that the $T(E)$ model includes the possibility of multiple reflections in the GaAs cap layer since $T(E_z,E_t)$ is calculated for the whole metal-heterostructure system. Since the GaAs cap layer is 100 Å thick, the effect of multiple reflections will be weak. Hence, the SK and $T(E)$ models give similar spectral shapes and second derivatives which resemble the heterostructure transmission probability.

To determine the band offsets, the single-barrier spectra were fit to the $T(E)$ model with ΔE_C and the amplitude factor R as the fitting parameters. The Schottky barrier was found by fitting the AL0 spectra and including the m-s transmission function (essentially the LP model). Thus, we fix the Schottky barrier and fit to the band offset directly. The results of the fits using the $T(E)$ model are shown in Fig. 5 for data taken at 77 K for the five compositions. The second thresholds from BK fits (not shown) were used as a guideline to determine the upper voltage limit for the single (Γ) valley $T(E)$ fits. The thresholds for the $T(E)$ model are relatively insensitive to fitting range as long as the range is not extended past the next threshold. The $T(E)$ fits generally show better agreement to the BEEM spectral shape at 77 K than

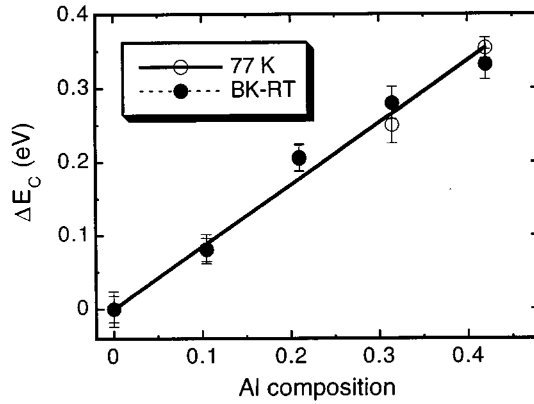

FIG. 6. RT and 77 K GaAs/$Al_xGa_{1-x}As$ conduction-band offsets (points) measured by BEES. Linear fits (lines) at both temperatures give $\Delta E_C = (0.84\ \text{eV})x$, or a fractional band offset of $Q_C = \Delta E_C / \Delta E_g = 0.68$. The linear curve fits and some data points are overlapping.

the BK fits. However, $T(E)$ and BK fits are almost indistinguishable at RT; the $T(E)$ model gives slightly lower thresholds as expected from the inclusion of the QM transmission probability.

The band offsets determined by BEEM at RT and 77 K are shown in Fig. 6. At some compositions the RT and 77 K measurements overlap obscuring one of the data points. Error bars are standard deviations from fitting at least 25 spectra at each composition and temperature. Linear fits (fixed at the origin) show an identical composition dependence of the band offset for 77 K and RT of $\Delta E_C = (0.84\ \text{eV})x$, or equivalently $\Delta E_C / \Delta E_g = 0.68$. This lack of T dependence was also found by Watanabe *et al.*[15] by C-V profiling on samples with $x \geqslant 0.2$. They could not measure 77 K band offsets for higher Al concentrations due to trapping of carriers by DX centers. BEEM measurements do not seem to be affected by this problem. Thus, we find good agreement with previous $Al_xGa_{1-x}As$/GaAs band offset measurements.[15,39]

VI. REVERSE BIAS DEPENDENCE

Although our heterostructures were engineered to have a flat band condition at RT, band bending can be induced by applying a base-collector bias to the structure. Since the energy distribution of the injected carriers is controlled by the tip-base bias, the heterostructure potential can now be tuned independently of the probe. In practice, applying a base-collector bias makes measurement of the BEEM current (~pA) difficult because this causes a "leakage" current which can be much larger than the BEEM current. However, BEEM with an applied reverse bias has been demonstrated in Au/Si Schottky diodes.[40] In this case, very small shifts in the BEEM threshold were observed since the applied bias drops across the long depletion region of the semiconductor. Both forward and reverse biases have been used to study transport through Si metal-oxide-semiconductor (MOS) structures.[41] The SiO_2 layer forms a large (~3 eV) potential barrier and gives a correspondingly small leakage current. Experiments on MOS structures require ultrahigh vacuum to achieve stable STM operation at tip biases >2 V.

The application of a reverse bias to single barrier

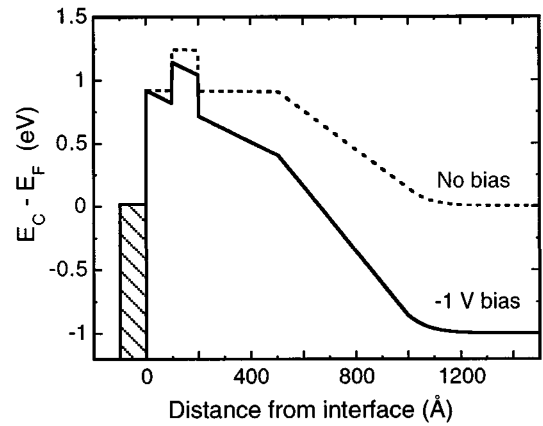

FIG. 7. Schematic band profiles for a single-barrier structure in equilibrium and under 1 V reverse bias. Note the reduction in barrier height for injected electrons under bias.

$Al_xGa_{1-x}As$ heterostructures forms an intermediate case with respect to the previous studies. The effect of applying a 1 V bias to the structure is illustrated schematically in Fig. 7. Since the structures have 1000 Å of undoped material between the metal (base) and the heavily doped substrate (collector), they will behave, to first order, as a capacitor. Except for a small change in the substrate depletion and the charge at the m-s interface, the applied bias should drop almost entirely over the undoped region. Under reverse bias, the effective barrier height should be lowered by approximately 10% of the applied bias because the potential maximum in the structure will be at the upper GaAs/$Al_xGa_{1-x}As$ interface. In principle, the $Al_xGa_{1-x}As$ barrier could be pulled below the Au-GaAs Schottky barrier with a large enough reverse bias.

Figure 8 shows the shift in the first (Γ) BEES threshold with applied reverse bias for an $Al_xGa_{1-x}As$ single-barrier sample with $x = 0.32$. The second threshold (not shown) also shifted to lower voltage with increasing reverse bias. The line in Fig. 8 is a calculation of the expected $Al_xGa_{1-x}As$ barrier height using $\Delta E_C = 0.65\ \ \Delta E_g$ and assuming a simple lever arm lowering of the potential. The measured shifts in the threshold give good agreement with this simple model.

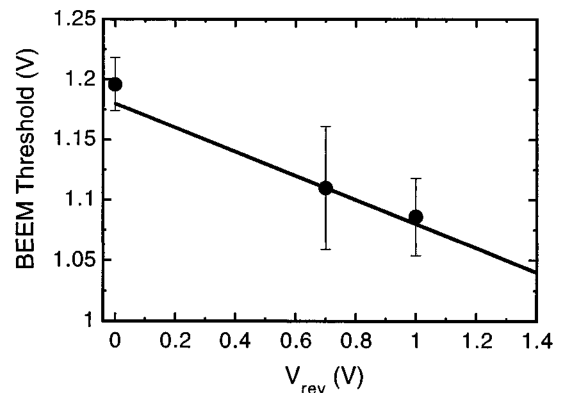

FIG. 8. Measured shift in BEES thresholds of $Al_xGa_{1-x}As$ ($x = 0.32$) barrier vs applied reverse bias. The line is a simple lever arm calculation of expected barrier lowering.

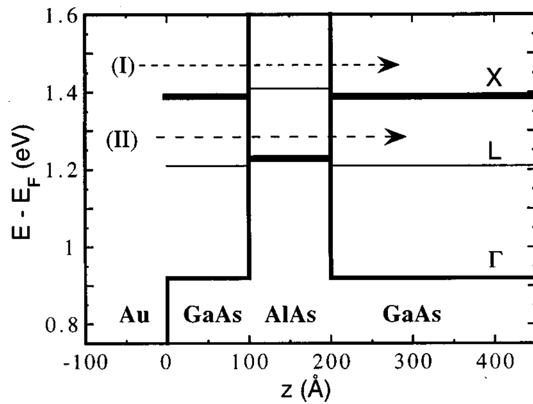

FIG. 9. Calculated RT 1D band profile for 100 Å AlAs single-barrier structure showing the positions of the Γ, *L*, and *X* minima. The AlAs Γ point is at ~2 eV. A strong BEES threshold is expected at 1.4 V from injection into the GaAs *X* valley (*X*-*X*-*X*) and transport over the AlAs *L* barrier (*L*-*L*-*L*) as indicated by arrow (I). Observation of a BEES threshold near 1.2 V would require coupling of Γ or *L* electrons in the GaAs cap layer into AlAs *X* quasibound states (Γ-*X*-Γ or *L*-*X*-*L* processes), shown as arrow (II).

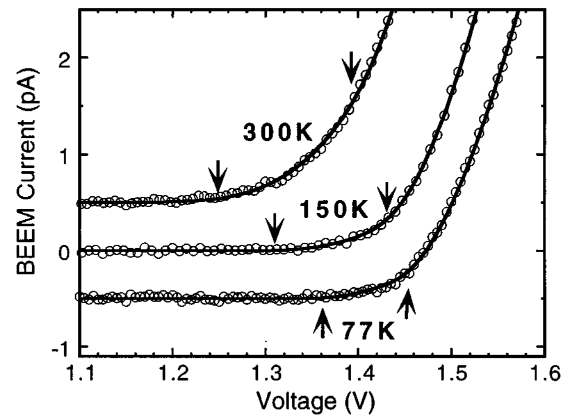

FIG. 10. *T* dependence of AlAs single-barrier BEES spectra. The strong threshold near 1.4 V due to GaAs *X* and AlAs *L* states shifts to higher energy at low *T* as expected. The weak current due to transport through AlAs *X* states shows a dramatic decrease in magnitude and increase in effective threshold (BK model) at low *T*.

This ability to apply a base-collector bias to a heterostructure while still retaining independent control over the injected electron energy distribution holds great promise for studying field-dependent hot carrier transport.

VII. INDIRECT $Al_xGa_{1-x}As$ BARRIERS

To this point, we have only discussed the behavior of single-barrier structures with Al compositions such that the lowest conduction-band minimum is at the zone center (Γ point). For Al compositions above 40–45 %, $Al_xGa_{1-x}As$ becomes indirect and its conduction-band minimum is located near the *X* point of the Brillouin zone. Since the GaAs *X* point is higher in energy than the $Al_xGa_{1-x}As$ *X* point, there will always be an effective potential well for *X* electrons in the 100 Å $Al_xGa_{1-x}As$ ''barrier'' in all of our structures (except AL0). The *X* states will only be quasibound since carriers can relax to lower-energy Γ or *L* states in the adjacent GaAs layers. For $x \geqslant 0.45$, these quasibound *X* states become the lowest energy levels in the $Al_xGa_{1-x}As$ layer. For example, a simple 1D potential diagram showing the Γ, *L*, and *X* point minima for an AlAs ($x=1$) single barrier is shown in Fig. 9. We have assumed a GaAs/AlAs valence-band offset of 0.44 eV for this calculation and used the AlAs band gaps from Ref. 23. An AlAs *L*-*X* separation of ~0.2 eV is expected and has been confirmed by Kaiser *et al.* in BEEM studies of GaAs capped with different thicknesses of AlAs.[7]

In our previous work on the DBRTS, peaks in second derivative BEEM spectra (which correspond to thresholds) were compared to the expected energy levels in the structure in order to identify the transport channels that contribute to the BEEM current.[10] At low *T*, weak structure was observed at energies that correspond to quasibound *X* states in the $Al_xGa_{1-x}As$ barriers. Considering that the DBRTS BEES spectra are a superposition of current contributions from several different transport channels, it is difficult to conclusively show that $Al_xGa_{1-x}As$ *X* states are responsible for the weak structure in the derivatives. In contrast, the AlAs single-barrier structure provides much clearer evidence for the transport process suggested in our DBRTS studies. Specifically, the observation of a threshold at ~1.2 V gives direct evidence of interband coupling from GaAs Γ (and possibly *L*) states in the cap layer into AlAs *X* states. Carriers must then be scattered back into GaAs Γ or *L* states to be collected. This Γ-*X*-Γ (or *L*-*X*-*L*) process is indicated by (II) in Fig. 9 and would be expected to give a weak current. For $V<1.4$ V, most of the injected carriers will be reflected at the GaAs/AlAs interface and fall back into the base. Aside from the intervalley current contribution, a strong threshold is expected at ~1.4 V due to the GaAs *X* band edge and injection over the AlAs *L* barrier. The GaAs *X* point and AlAs *L* point are almost degenerate so only one threshold will be observed from these two transport channels (*X*-*X*-*X*, *L*-*L*-*L*) which are indicated by (I) in Fig. 9.

Figure 10 shows the temperature dependence of BEES spectra from the AlAs single-barrier structure. At RT, a strong threshold is observed as expected at 1.40 V, indicated by an arrow in Fig. 10. At lower voltages, a weaker current is found which turns on at 1.24 V, in good agreement with the expected energy of the AlAs *X* band edge. Threshold values were determined by simple fits to the BK model assuming two band contributions. Fitting to a single-band (GaAs *X*) model fails to accurately reproduce the shape of the BEES spectra between 1.2 and 1.4 V at RT. As seen in Fig. 10, the spectral shape changes significantly at lower *T*. The strong threshold at 1.4 V moves to higher energy as expected from the *T* dependence of the energy gaps. However, the weak current associated with the AlAs *X* states shows an anomalous threshold shift to higher voltage as well as a marked reduction in magnitude relative to the GaAs *X* current. The shift in apparent threshold with *T* is illustrated in Fig. 11 where the BEEM thresholds are compared to the expected *T* dependence of the GaAs *X* and AlAs *X* points. Note that the second threshold follows the GaAs *X* band edge quite well, but the first threshold diverges from the expected AlAs *X* point. For this calculation we use the *T* dependence of the Au/GaAs Schottky barrier which we have measured by BEEM and assume the bands follow the Varshni equation

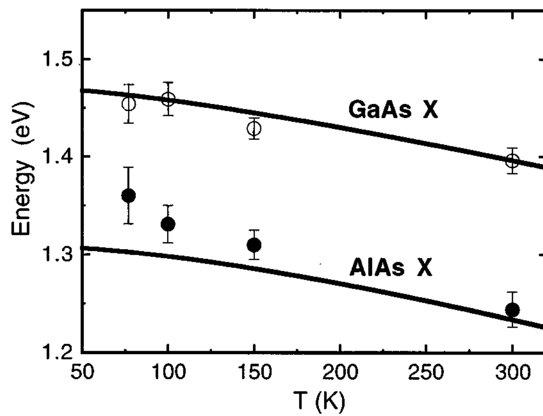

FIG. 11. T dependence of AlAs single-barrier BEES thresholds (points) and calculated positions of GaAs and AlAs band edges (lines). Note that at low T the first threshold which is due to intervalley scattering diverges from expected energy of the AlAs X minima.

using the coefficients of Aspnes.[42]

Although the two-valley BK model provides a good fit to the data, it was used primarily as a consistent procedure to determine an effective threshold. Hence, the shift in the apparent AlAs X-related threshold should not be interpreted as a shift in the energy level with T. The shift is much larger than the 30 meV increase in the GaAs/AlAs (Γ-X) band offset predicted theoretically.[43] The reduction in the magnitude of the intervalley current should be interpreted as a change in the intervalley scattering processes with T. Thus, we need to examine the possible mechanisms for intervalley transfer and determine which are consistent with our observed T dependence. Γ-X intervalley transfer in GaAs/$Al_xGa_{1-x}As$ has been investigated experimentally[44,45] and theoretically.[46–48] Conservation of k_t is typically assumed for the epitaxial GaAs/AlAs interface. Most generally, transfer into both the on-axis X_z and lateral $X_{X,Y}$ minima must be considered. Γ-X_Z-Γ coupling is intrinsically possible since the AlAs X_Z and GaAs Γ bands overlap in the interface Brillouin zone and can satisfy k_t conservation. Transfer into the lateral minima ($X_{X,Y}$) requires additional transverse momentum which can be provided by phonon scattering or by alloy disorder scattering, as pointed out by Price.[47] Although alloy disorder is not relevant for AlAs, one could argue that scattering from interface roughness could provide the extra k_t.

In principle, another possible mechanism in the BEES experiment would be tunneling through the GaAs cap layer directly into an AlAs X state. However, for a 100 Å cap layer with a large (GaAs X) effective mass, the tunneling probability will be very low and would not be T dependent. Assuming the lateral spread of the injected electron distribution does not change much with T, the coherent Γ-X_Z-Γ process will not be T dependent. Interface disorder scattering will also not change with measurement T. Therefore, we conclude that the reduction in the AlAs X-related current is caused by the reduction of the phonon population (which affects both phonon emission and absorption) at low T. In fact, one could argue that excess current is observed at high T due to the additional scattering processes and that the low T spectra provide a better measure of the strength of the Γ-X_Z coupling.

A similar argument was used by Bell *et al.* to explain an anomalous T dependence of attenuation lengths measured by BEEM on (100)Si *pn* junctions.[6] Longer attenuation lengths were found at 300 K than at 77 K. Since the off-axis $X_{X,Y}$ minima have a smaller mass in the transport direction than the X_Z minima, a higher electron population in the off-axis minima at high T (due to phonon scattering) gives on average a longer attenuation length. Note that the symmetry of Si and AlAs are similar; both have their absolute conduction-band minima near the X point. In Si, the intervalley scattering is between X_Z and $X_{X,Y}$ states, both of which can contribute to the BEEM current. In the GaAs/AlAs single barriers, two scattering events are required to produce BEEM current. The first (Γ,L)-X scattering allows the carrier to enter an AlAs X quasibound state and another X-(Γ,L)scattering is required for the electron to escape the well and be collected in the substrate. Some carriers which reach the AlAs X well are scattered back into the GaAs cap layer and then swept out the base and therefore do not contribute to the BEEM current.

Although the 100 Å AlAs layer will give quantization of the z energy, subbands will not be resolvable in the BEEM spectra. In principle the X_Z states (along the growth direction) and the lateral $X_{X,Y}$ states will be nondegenerate because they have a different effective mass along the confinement direction. However, the level splitting will be <10 meV and should also not be resolvable by BEEM at 77 K. Thus, quasiconfinement effects can be neglected. Recent work by Westwood *et al.* in similar structures to those studied here reported no discernible differences between BEEM spectra of 100 and 300 Å AlAs barriers capped by 100 Å GaAs.[49] Our RT thresholds are in good agreement with their results. However, they were unable to elucidate the intervalley scattering mechanisms since their measurements were only performed at RT.

We would like to emphasize the importance of the GaAs X point in the interpretation of the BEEM spectra when a GaAs cap layer is present. For the AlAs single barrier, the second strong threshold is due to the combined contributions of carriers in the L and X channels. In Ref. 37, the second BEEM threshold for a 100 Å GaAs–300 Å AlAs structure was attributed solely to the AlAs L point. In fact, if the AlAs L point was much higher in energy, a strong threshold near 1.4 V would still be observed since electrons injected over the Schottky barrier into the GaAs X valley will be collected with high probability. We expect two different thresholds due to the GaAs X point and AlAs X states because these currents have different transport mechanisms. In the case of the 50 ml thick AlAs cap layer studied by Kaiser *et al.*,[7] the BEEM spectra will reflect the AlAs bulk-band structure only, and the GaAs X point should not play a role.

We have also studied an $Al_xGa_{1-x}As$ single barrier with $x=0.7$. This sample also shows the weak intervalley current and a two threshold behavior with thresholds similar to the AlAs values at RT. Considering that the $Al_xGa_{1-x}As$ L barrier will be lower for $x=0.7$, one would expect the second threshold to shift slightly to lower energy—if the L current was the dominant contribution to this threshold. This is not

TABLE I. RT BEEM thresholds from two band BK fitting and resulting conduction band offsets.

% Al	Fit range (V)	First band	V_1 BK fit (V)	Second band	V_2 BK fit (V)	ΔE_C (eV)
0.0	0.8–1.4	GaAs Γ	0.915±0.018	GaAs *L*	1.212±0.012	
0.11	0.9–1.4	$Al_xGa_{1-x}As$ Γ	0.992±0.013	$Al_xGa_{1-x}As$ *L*	1.260±0.015	0.077
0.21	1.0–1.5	$Al_xGa_{1-x}As$ Γ	1.121±0.019	*L* & *X*	1.328±0.010	0.206
0.32	1.0–1.6	$Al_xGa_{1-x}As$ Γ	1.196±0.022	*L* & *X*	1.356±0.016	0.281
0.42	1.1–1.6	$Al_xGa_{1-x}As$ Γ	1.249±0.020	GaAs *X*	1.369±0.021	0.334
0.70	1.1–1.7	$Al_xGa_{1-x}As$ *X*	1.252±0.029	GaAs *X*	1.420±0.019	0.337
1.0	1.1–1.7	AlAs *X*	1.244±0.018	GaAs *X*	1.397±0.013	0.329

observed which further supports the importance of the GaAs *X* contribution to the BEEM current.

VIII. SUMMARY OF BAND-STRUCTURE EFFECTS

The composition dependence of the RT BEES thresholds observed for all samples studied are plotted in Fig. 12 along with the expected $Al_xGa_{1-x}As$ band-edge positions. The band minima were referenced to the Au/GaAs Schottky barrier to enable direct comparison with the BEES thresholds. The band-gap relations were taken from Ref. 23, and the 65/35 Γ band offset rule for the direct gap regime was extrapolated to the whole composition range. As shown in Fig. 4, the two threshold BK fits reproduce the spectral shape very well at RT. In fact, the line shapes of the Γ current of the BK and $T(E)$ fits are indistinguishable at RT. Further, the band offset values obtained from the two threshold BK fits were almost identical to those obtained from the $T(E)$ fits. This gives us confidence in using the BK fits as a consistent procedure for assigning higher thresholds to the RT spectra.

A summary of the threshold values and fitting ranges is given in Table I. To reduce the number of fitting parameters, initially only two threshold contributions were considered, and the fitting ranges were selected appropriately. For example, the AL0 data were initially fitted assuming contributions of the Γ and *L* valleys over the voltage range 0.8–1.4 V. When only two valleys were considered, the fits were cut off at 1.4 V because an additional current is found at this voltage due to injection into the GaAs *X* valley. Extending the fitting range to 1.6 V enables the identification of the third (GaAs *X*) threshold for both the $x=0$ and 0.11 data. The results from these three band fits for these two compositions are shown in Fig. 12.

As seen in Fig. 12, the $Al_xGa_{1-x}As$ Γ, *L*, and *X* minima converge as the Al composition approaches 0.45. For $x=0.21$ and 0.32, only two components were included in the fits because the *L* and *X* points are too close in energy to be resolved. So, the second threshold for these two compositions (open circles in Fig. 12) represents an average of the expected $Al_xGa_{1-x}As$ *L*, $Al_xGa_{1-x}As$ *X*, and GaAs *X* thresholds. For $x=0.42$, the first BEES threshold is due to the combined contributions of the $Al_xGa_{1-x}As$ Γ, *L*, and *X* channels. This is noticeable in Fig. 5 where the $T(E)$ fit for $x=0.42$ shows a larger contribution to the total BEEM current compared to the fits for the lower concentrations. The second, strong threshold near 1.4 V is also observed for $x=0.42$ due to the GaAs *X* minima as discussed extensively in the previous section. The two thresholds observed for each of the $x=0.7$ and 1 single barriers are also shown in Fig. 12.

In conclusion, we have presented a systematic BEES study of $Al_xGa_{1-x}As$ single-barrier heterostructures. Samples were designed to obtain a uniform, reproducible Au/GaAs interface which provides an internal energy reference for the heterostructure experiments. For single $Al_xGa_{1-x}As$ barriers in the direct regime, the shift in the initial (Γ) threshold gives good agreement with the GaAs/$Al_xGa_{1-x}As$ conduction-band offsets measured by other techniques. Using *T*-dependent BEES, we have identified phonon scattering as the dominant intervalley scattering process which contributes to BEEM current through indirect $Al_xGa_{1-x}As$ barriers. Finally, good agreement between BEES thresholds and the expected $Al_xGa_{1-x}As$ Γ, *L*, and *X* band minima was found over the entire composition range. This comprehensive study of the prototypical GaAs/$Al_xGa_{1-x}As$ system has demonstrated the capability of BEES to accurately probe semiconductor band structure. With its unique combination of excellent lateral resolution and energy spectroscopy, BEEM promises to continue providing new information about quantum structures and semiconductor transport properties.

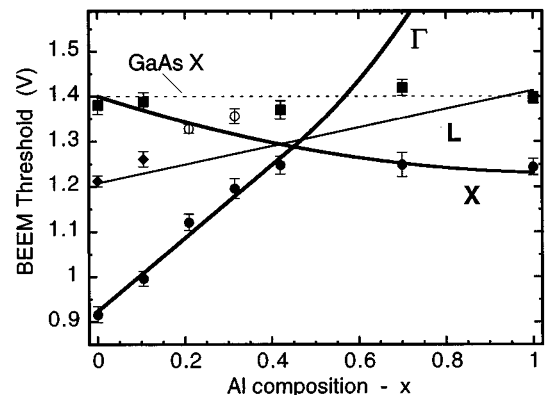

FIG. 12. Summary of RT BEES thresholds (points) for 100 Å $Al_xGa_{1-x}As$ single-barrier heterostructures. Lines show the composition dependence of band minima assuming a linear valence-band offset, $\Delta E_V=(0.44\ \text{eV})x$, using the band-gap relations of Ref. 23. Good agreement with the $Al_xGa_{1-x}As$ absolute conduction-band minimum (filled circles), the $Al_xGa_{1-x}As$ *L* point (filled diamonds) and the GaAs *X* point (filled squares) is found. For $x=0.21$ and 0.32, the second BEES threshold (open circles) represents an average of the *L* and *X* band contributions.

ACKNOWLEDGMENTS

We thank D. B. Leonard, G. Medeiros-Ribeiro, and J. P. Ibbetson for MBE growth of samples. We acknowledge stimulating discussions with D. L. Smith (Los Alamos National Laboratory) and T. Sajoto. J.J.O'S would like to thank Professor A. C. Gossard for encouragement. This work was supported by AFOSR Grant No. F49620-94-1-0378, NSF Grant No. ECS-9531133, and the Midwest Research Institute NREL Contract No. SCR-6-16770. E.G.B. acknowledges support from Los Alamos National Laboratory under CULAR Grant No. STBLUC: 95-141 (CULAR). M.E.R. was supported by QUEST, a NSF Science and Technology Center.

*Electronic address: venky@engineering.ucsb.edu

[1] G. Binning, H. Rohrer, C. Gerber, and E. Weibel, Phys. Rev. Lett. **49**, 57 (1982).

[2] L. D. Bell and W. J. Kaiser, Phys. Rev. Lett. **61**, 2368 (1988).

[3] W. J. Kaiser and L. D. Bell, Phys. Rev. Lett. **60**, 1406 (1988).

[4] G. N. Henderson, T. K. Gaylord, E. N. Glytsis, P. N. First, and W. J. Kaiser, Solid State Commun. **80**, 591 (1991).

[5] R. H. Williams, Appl. Surf. Sci. **70/71**, 386 (1992).

[6] L. D. Bell, S. J. Manion, M. H. Hecht, W. J. Kaiser, R. W. Fathauer, and A. M. Milliken, Phys. Rev. B **48**, 5712 (1993).

[7] W. J. Kaiser, M. H. Hecht, L. D. Bell, F. J. Grunthaner, J. K. Liu, and L. C. Davis, Phys. Rev. B **48**, 18 324 (1993).

[8] L. D. Bell, A. Milliken, S. J. Manion, W. J. Kaiser, R. W. Fathauer, and W. T. Pike, Phys. Rev. B **50**, 8082 (1994).

[9] J. J. O'Shea, T. Sajoto, S. Bhargava, D. Leonard, M. A. Chin, and V. Narayanamurti, J. Vac. Sci. Technol. B **12**, 2625 (1994).

[10] T. Sajoto, J. J. O'Shea, S. Bhargava, D. Leonard, M. A. Chin, and V. Narayanamurti, Phys. Rev. Lett. **74**, 3427 (1995).

[11] E. Y. Lee, S. Bhargava, K. Luo, M. A. Chin, and V. Narayanamurti, Appl. Phys. Lett. **69**, 940 (1996).

[12] J. J. O'Shea, C. M. Reaves, S. P. DenBaars, M. A. Chin, and V. Narayanamurti, Appl. Phys. Lett. **69**, 3022 (1996).

[13] M. E. Rubin, G. Medeiros-Ribeiro, J. J. O'Shea, M. A. Chin, E. Y. Lee, P. M. Petroff, and V. Narayanamurti, Phys. Rev. Lett. **77**, 5283 (1996).

[14] S. Bhargava, H.-R. Blank, V. Narayanamurti, and H. Kroemer, Appl. Phys. Lett. **70**, 759 (1997).

[15] M. O. Watanabe, J. Yoshida, M. Mashita, T. Nakanisi, and A. Hojo, J. Appl. Phys. **57**, 5340 (1985).

[16] J. Batey and S. L. Wright, J. Appl. Phys. **59**, 200 (1986).

[17] J. G. Simmons, J. Appl. Phys. **34**, 1793 (1963).

[18] R. Ludeke and M. Prietsch, J. Vac. Sci. Technol. A **9**, 885 (1991).

[19] D. L. Smith and S. M. Kogan, Phys. Rev. B **54**, 10 354 (1996).

[20] E. O. Kane, J. Appl. Phys. **32**, 83 (1961).

[21] G. L. Snider, 1D Poisson/Schroedinger Solver ver. 2.1.3.

[22] Surface/Interface, Inc., Mountain View, CA 94041.

[23] S. Adachi, J. Appl. Phys. **58**, R1 (1985).

[24] M. H. Hecht, L. D. Bell, and W. J. Kaiser, Appl. Surf. Sci. **41/42**, 17 (1989).

[25] W. J. Kaiser, L. D. Bell, M. H. Hecht, and F. J. Grunthaner, J. Vac. Sci. Technol. B **7**, 945 (1989).

[26] A. E. Fowell, R. H. Williams, B. E. Richardson, A. A. Cafolla, D. I. Westwood, and D. A. Woolf, J. Vac. Sci. Technol. B **9**, 581 (1991).

[27] A. A. Talin, D. A. Ohlberg, R. S. Williams, P. Sullivan, I. Koustelas, B. Williams, and K. L. Kavanagh, Appl. Phys. Lett. **62**, 2965 (1993).

[28] A. A. Talin, R. S. Williams, B. A. Morgan, K. M. Ring, and K. L. Kavanagh, Phys. Rev. B **49**, 16 474 (1994).

[29] S. Bhargava, T. Sajoto, J. J. O'Shea, M. A. Chin, and V. Narayanamurti (unpublished).

[30] J. R. Waldrop, Appl. Phys. Lett. **44**, 1002 (1984).

[31] L. D. Bell, M. H. Hecht, and W. J. Kaiser, Phys. Rev. Lett. **64**, 2679 (1990).

[32] M. H. Hecht, L. D. Bell, W. J. Kaiser, and L. C. Davis, Phys. Rev. B **42**, 7663 (1990).

[33] H. Palm, M. Arbes, and M. Schulz, Phys. Rev. Lett. **71**, 2224 (1993).

[34] J. P. Sullivan, R. T. Tung, F. Schrey, and W. R. Graham, J. Vac. Sci. Technol. A **10**, 1959 (1992).

[35] J. S. Blakemore, J. Appl. Phys. **52**, R123 (1982).

[36] A. E. Fowell, A. A. Cafolla, B. E. Richardson, T. H. Shen, M. Elliott, D. I. Westwood, and R. H. Williams, Appl. Surf. Sci. **56-58**, 622 (1992).

[37] M. Ke, D. I. Westwood, C. C. Matthai, B. E. Richardson, and R. H. Williams Phys. Rev. B **53**, 4845 (1996).

[38] The dark areas are always correlated with sharp spikes in the STM image in the scanning direction. They are generally reproducible in consecutive images of the same area. These instabilities can be explained by adsorbates (dirt) on the surface. When the STM tip encounters a ''dirty'' area, the tip sticks to the adsorbates, the tunneling process is disrupted, and the apparent tunneling current increases. In response, the feedback pulls the tip out which explains the spikes in the STM topography and the absence of measured BEEM current. Images taken with a lower tunneling current setpoint at the same bias voltage show fewer of these instabilities. This is consistent with the larger average tip-sample spacing for a lower setpoint.

[39] H. Okumura, S. Misawa, S. Yoshida, and S. Gonda, Appl. Phys. Lett. **46**, 377 (1985).

[40] A. Davies and H. G. Craighead, Appl. Phys. Lett. **64**, 2833 (1994).

[41] R. Ludeke, A. Bauer, and E. Cartier, J. Vac. Sci. Technol. B **13**, 1830 (1995).

[42] D. E. Aspnes, Phys. Rev. B **14**, 5331 (1976).

[43] K. J. Malloy and J. A. VanVechten, J. Vac. Sci. Technol. B **9**, 2212 (1991).

[44] P. M. Solomon, S. L. Wright, and C. Lanza, Superlattices Microstruct. **2**, 521 (1986).

[45] E. E. Mendez, E. Calleja, C. E. T. G. da Silva, L. L. Chang, and W. I. Wang, Phys. Rev. B **33**, 7368 (1986).

[46] H. C. Liu, Appl. Phys. Lett. **51**, 1019 (1987).

[47] P. J. Price, Surf. Sci. **196**, 394 (1988).

[48] Z. S. Gribnikov and O. E. Raichev, Fiz. Tek. Poluprovodn. **23**, 2171 (1989) [Sov. Phys. Semicond. **23**, 1344 (1989)].

[49] D. I. Westwood, M.-L. Ke, F. Lelarge, F. Laruelle, and B. Etienne, Surf. Sci. **352-354**, 802 (1996).